Journal of Building Engineering 64 (2023) 105606

Contents lists available at ScienceDirect

Journal of Building Engineering

journal homepage: www.elsevier.com/locate/jobe

Flexural behaviour of a new timber-concrete composite structural flooring system. Full scale testing

Emilio Martín-Gutiérrez *, Javier Estévez-Cimadevila, Félix Suárez-Riestra, Dolores Otero-Chans

University of Coruña, Architectural Structures Research Team, Center for Technological Innovation in Construction and Civil Engineering, Spain

ARTICLE INFO

Keywords:
Timber-concrete composite
Timber flooring systems
Flexural behaviour
Four-point bending test

ABSTRACT

Timber-concrete composite systems are a high-performance alternative for building floors, of great interest in the current context of environmental concerns. Looking for a more eco-friendly solution, the paper presents a new flooring system with a wood-concrete connection that does not require adhesives or special metal elements. Four-point bending tests were performed on TCC flooring samples with a span of 6.0, 7.2 and 8.4 m. Its cross section was a prefabricated piece in the shape of an inverted T made up of a lower glulam flange, glued together with a central plywood rib with aligned holes in its upper part that go through the entire thickness of the plywood. The set was completed with a top layer of poured-in-place concrete. The connection between both materials is achieved by penetrating the concrete into the rib holes. Additionally, corrugated steel bars were placed through said holes to achieve ductile behaviour. In all cases, a slenderness ratio of L/24 was used. The experimental results showed that the lowest value of ultimate load obtained was 4.3 times higher than the total service load estimated for a building for public use (9 kN/m^2). The maximum deflection of the total load was between L/573 and L/709 for the loads corresponding to a building for public use (9 kN/m^2) and between L/1069 and L/1340 for the case of residential type building (5 kN/m^2). An analysis of the effects of vibrations in the service limit state in relation to user comfort has been included. The results indicate that the system satisfies the requirements for the intended uses.

Consequently, the proposed solution shows its effectiveness both in terms of strength and stiffness for the construction of light floors, being easy to build and having high performance.

1. Introduction

Evidence of climate change and increasing environmental degradation call for urgent global action. It is estimated that in 2015 buildings were responsible for 38% of CO_2 emissions related to energy demand [1]. Even though this figure in 2020 was reduced by the effect of the global pandemic, new increases are expected related to economic recovery, demographic growth, and the massive exodus to the cities [2]. In this context, studies on the life cycle assessment of buildings proliferate, covering all possible stages (construction, operating, maintenance, repair, replacement, refurbishment, demolition, waste processing) [3–6]. The goal is to develop more eco-friendly strategies.

In Europe, public institutions have directed a large part of their resources to the improvement of building envelopes and the

* Corresponding author.
E-mail address: emilio.martin@udc.es (E. Martín-Gutiérrez).

https://doi.org/10.1016/j.jobe.2022.105606
Received 14 July 2022; Received in revised form 13 November 2022; Accepted 22 November 2022
Available online 25 November 2022

production of renewable energy [7,8]. The other focus of attention is the construction materials and systems [9–11]. Consequently, the use of wood has increased notably due to its well-known benefits (fundamentally, thermal properties, embodied carbon, and recycling) [12,13]. In the case of large-span floors having the stiffness as a key design factor, some only-timber solutions have been studied that combine structural efficiency with a competitive economic cost, although results are still limited [14]. Commercial systems, such as the so-called Kielsteg, allow spans of up to 28 m with span/height ratios around 30 [15]. However, the possible deforestation associated with excessive demand, or the trend towards monoculture of certain species, is also a cause for concern [16,17]. Timber-concrete composite (TCC) systems aim to provide an answer to this question, so that the combination of materials allows a better use of them and consequently a reduction in resource consumption [18–20]. Likewise, and in reference to the structural behaviour, the TCC solutions present greater stiffness and better behaviour against fire than the only-timber ones, and are lighter than the conventional ones with massive use of concrete.

Wooden materials more used TCC floors has been glulam (glued laminated timber) [21–27] and, recently, CLT (cross laminated timber) [28–30], although systems based on saw timber or LVL (laminated veneer lumber) can also be found [31–33]. Glulam has the advantage of being an inexpensive and well-known material that is easily available for medium span lengths such as those used in the proposed solution.

Referring to the topping concrete slab, both the use of conventional reinforced concrete (i.e. concrete reinforced with rebars) [21,24–26,34] and fibre reinforced concrete [27,35,36] have been broadly studied. When notches are used, the strength of the concrete can become a key factor in the behaviour of the system [37]. However, in other comparative studies governed by wood failure the types of concrete used did not show significant differences in the behaviour of the system [38]. Some studies using Ultra-High Performance Fiber Reinforced Concrete have shown that allows to reduce the thickness of the slab, and therefore the self-weight of the solution, and the creep deflections [39,40].

Shear connection devices are crucial in any mixed system. Its effectiveness increases by reducing the relative slippage between components, achieving an adequate composite action. Other requirements to consider are strength, stiffness, and ductility. There is a wide variety of connection solutions, which are usually organised into three categories, based on the criteria of Kanócz et al.: screwed [35], grooved [36], and adhesive connections [28].

The first group comprises any type of steel fasteners, including screws in different arrangements [21,22,29,41–43], bolts or threaded bars [23,34,44–46], steel plates [24,30,31], or more complex designs [25,47]. The second category includes notches or slots made in wood [40,48], frequently combined with metallic elements [26,32,49–51]. The last group corresponds to solutions with adhesives, either directly between wood and concrete [33,52,53], or by gluing metal bars or plates [27,54]. Steel elements, whether they are pins, bars or plates, have the material advantages of well-known behaviour and its plastic stage that facilitates the design of systems with ductile failure modes. When using steel bars, rebars offer also an unexpensive solution. Notched solutions allow the design of systems with high strength and stiffness, but can experiment brittle failure. For this reason, in many cases solutions have been used that combine fasteners and notches, obtaining solutions with high strength and ductile failures due to the plasticization of the fasteners. Despite that more sustainable structural adhesives are being developed, currently solutions with adhesives are less sustainable and less economical than other solutions.

On this basis, towards sustainability, a system is proposed with the aim of limiting the use of structural adhesives and steel elements. At the same time, constructability and easy of assembly were also concerns take into account. In this line, the research by Daňková et al. [55] constitutes a unique reference case, by using a glued-in board made of beech plywood as a connection element. It features longitudinal grooves in its lower part to improve adhesion to the glulam rib and holes in the upper part to facilitate rebar placement and concrete penetration. They tested three full-scale samples with 6.5 m span and 370 mm height. Different levels of

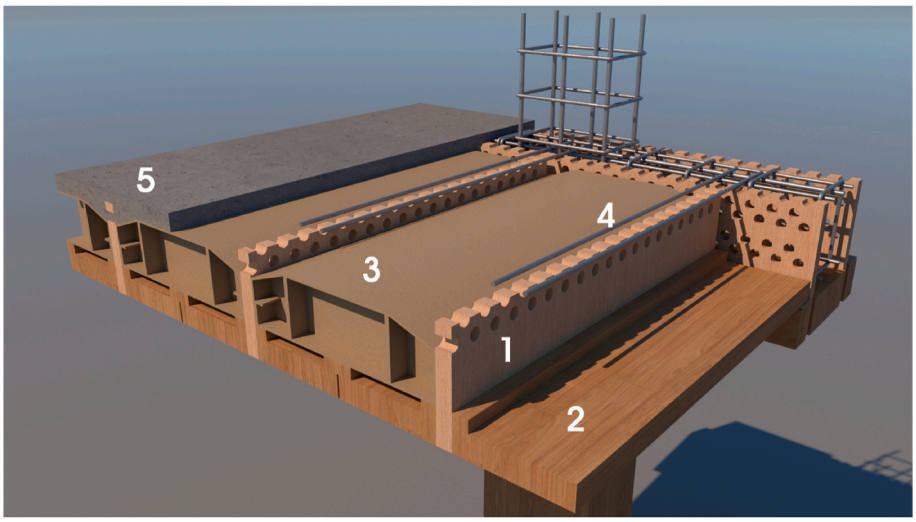

Fig. 1. Three-dimensional model. Components of the flooring system: 1 plywood rib, 2 glulam flange, 3 in-fill blocks, 4 rebars, 5 concrete slab.

environmental effects are applied to the samples, but they conclude that a good composite action is achieved in all cases. Plywood is also a readily available material, as well as glulam, and from Ref. [55] a ductile failure of the connection can be expected from using perforated plywood as shear connector.

2. Background

Our team has developed a comprehensive construction system, with TCC sections (Fig. 1), protected by the Spanish Office of Patents and Brands under reference ES1242743. Floors and beams are prefabricated pieces with inverted T- or π-shape sections, with a glulam flange and board ribs made of perforated plywood. Perforated boards act as continuous connectors with the top layer of poured-in-place concrete. This means that no gluing is required after the lamination process to achieve a connection between the ribs and the concrete. The only additional elements to have before pouring are the in-fill blocks and the reinforcements bars. The first can be marketed models of expanded polystyrene (EPS) or recycled materials, or specific designs made with cardboard. The second include transversal steel bars, housed in the holes of the plywood to improve the ductility of the connection, the steel mesh in the upper slab to control shrinkage, and the reinforcement bars necessary to resist the negative bending moments on the supports of the continuous pieces.

Previous phases of the investigation included three experimental campaigns: delamination test of the glued interfaces, shear test along the glue line, and shear test of the timber-concrete connection [56,57]. The results obtained ratify the viability of the system and the proper behaviour of the connection, in terms of strength, stiffness, ductility and composite action. Likewise, an analytical study has been carried out on the behaviour of the proposed flooring system, to determine possible areas of use and pre-dimensioning criteria [56]. This paper describes the four-point bending tests carried out with pieces between 6.0 and 8.4 m of span. The results are compared with previous estimates and analysed in order to facilitate the practical applicability of the system.

3. Materials and methods

3.1. Specimens

Nine specimens were prepared for the bending tests, three samples for each of the span lengths (L) considered: 6.0, 7.2 and 8.4 m. The floor thicknesses used were, respectively, 25, 30 and 35 cm, corresponding to a slenderness ratio of L/24. This pre-dimensioning is adjusted to the previous analytical study [56], in which a permanent load (in addition to its self-weight) of 2.0 kN/m^2 was considered, and another variable of 5.0 kN/m^{2,} both in service values. This data corresponds to the use category C5 defined in Eurocode 1 [58], valid for public access areas.

The prefabricated wooden pieces had an inverted T section and are made up of a 60 mm thick glulam flange made with *Picea abies*, with a strength class GL24h GLT [59]. In the area of contact with the plywood board, the thickness of the flange was increased to 90 mm in order to reduce shear stresses in the glue line between both materials (plywood and GLT) (Fig. 2). The assembly was formed in a laminating press using polyurethane adhesive (PUR) (Fig. 3, upper left).

A 40 mm thick birch plywood board was used as a wood-concrete connection with the distribution of perforations shown in Fig. 2. Every three perforations (186 mm) a transverse corrugated bar of 8 mm diameter, 120 mm long and quality B500S, according to UNE 36068:2011 [60], was inserted. As can be seen in Fig. 3, the rib is not required to be one continuous piece over the entire length of the span. The specimens have been manufactured with two discontinuities in the rib. This issue could facilitate the application of a precamber to compensate for deflections due to self-weight or shortening caused by concrete shrinkage.

In-fill blocks with internal ribs and folds were designed as lightning elements to provide them with the necessary stiffness during the construction process.

The upper concrete slab is made with CEM II/A-M (V-L) 42.5 R cement [61], with a content of 360 kg/m^3 Sikafiber Force M − 48 polyolefin macrofibres added (48 mm long, 465 N/mm^2 tensile strength), according to EN 14889–2:2006 [62], at a proportion of 4% in order to improve cracking behaviour caused by shrinkage. Additionally, a 200 × 200 mm steel mesh with quality B500S 6 mm diameter bars was placed. Likewise, two 10-mm reinforcement steel bars were placed at the ends of all the pieces for future negative

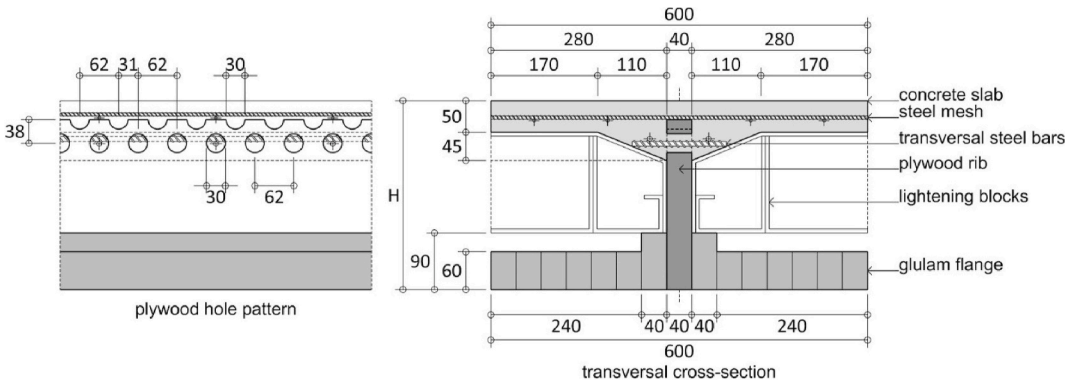

Fig. 2. Geometric parameters of the test specimen. Dimensions in mm.

Fig. 3. Stages of specimens' manufacture.

bending tests as cantilever beams, according to the test planning described in section 3.2. Compression tests were carried out according to EN 12390–3:2009 [63], obtaining an average strength at 28 days of 39.9 N/mm^2.

Table 1 summarizes the mechanical parameters of the materials used, while Table 2 shows the characteristics of the specimens. These were stored under standard conditions of temperature and humidity until stabilization. The relative humidity indicated in Table 2 is the average value obtained with a GANN Hydromette RTU 600 at two points in the glulam, before placing the specimen in the test area.

Before the start of the tests (Fig. 3, lower right), the glulam flange and the concrete slab were wedged using pieces of wood in the support and load application areas. The objective was to avoid any possible torsional effects caused by accidental eccentricities during the test, which could not occur in a floor with multiple ribs.

3.2. Test setup

Four-point bending tests were performed according to standard EN 408:2010 + A1:2012 [64], with a PB2–F/600 Micro test

Table 1
Mechanical parameters of the materials.

Birch plywood (manufacturer specifications | WISA® plywood)																			
Nominal thickness [mm]		Number of piles		Characteristic compression strength [N/mm^2]		Mean MOE in compression and tension [N/mm^2]		Characteristic panel shear [N/mm^2]		Characteristic planar shear [N/mm^2]		Mean MOR in panel shear [N/mm^2]		Mean MOR in planar shear [N/mm^2]	
				$f_{c,0}$	$f_{c,90}$	$E_{t,c,0}$	$E_{t,c,90}$	$f_{v,0}$	$f_{v,90}$	$f_{r,0}$	$f_{r,90}$	$G_{v,0}$	$G_{v,90}$	$G_{r,0}$	$G_{r,90}$
40		29		26.5	25.5	8925	8575	9.5		2.6	2.4	620		205	180
Glulam GL24h (EN 14080:2013)																			
Characteristic bending strength [N/mm^2]		Characteristic tensile strength [N/mm^2]		Characteristic compression strength [N/mm^2]		Characteristic shear strength [N/mm^2]		Mean Modulus of Elasticity [N/mm^2]		Mean Shear Modulus of Elasticity [N/mm^2]		Characteristic density [kg/m^3]		Mean density [kN/m^3]	
$f_{m,k}$		$f_{t,0,k}$	$f_{t,90,k}$	$f_{c,0,k}$	$f_{c,90,k}$	$f_{v,k}$		$E_{0,mean}$	$E_{90,mean}$	G_{mean}		ρ_k		ρ_{mean}	
24		19.2	0.5	24	2.5	3.5		11500	300	650		385		420	
Corrugated steel bars B500S (UNE 36068:2011)																			
Yield strength [N/mm^2]				Ultimate tensile strength [N/mm^2]						Ultimate strain [%]									
f_y				f_u						ε_u									
≥500				≥550						≥5.0									
Fiber-reinforced concrete (EN 12390–3:2009)																			
Age [days]				Mean density [kg/m^3]						Mean compression strength [N/mm^2]									
28				2355						39.9									

Table 2
Characteristics of the specimens.

Designation	Height H [mm]	Total length L_t [mm]	Span L [mm]	Average humidity in specimen [%]
250.1	250	6150	6000	14.9
250.2				14.4
250.3				14.6
300.1	300	7350	7200	15.3
300.2				15.4
300.3				14.6
350.1	350	8600	8400	15.3
350.2				15.7
350.3				15.6

hydraulic machine, whose load capacity is 600 kN (Fig. 4). Vertical displacement at midspan were measured using a Schreiber SM160.100.2.ST inductive displacement transducer with 100 mm of standard measurement stroke. On the lower flange, and on both sides of the plywood rib, rigid aluminium bars with a central transducer have been arranged in order to determine the stiffness of the piece in the area not subjected to shear stress (L_1). In addition, an Aramis 3D sensor was used to apply Digital Image Correlation (DIC) to analyse displacements and strains without contact (Fig. 5).

The effective bending stiffness was calculated using equations (1) and (2), the first corresponding to the central area subjected to pure bending (local MOE), and the second to a global estimate of the entire piece (global MOE).

$$EI_{t,L1} = \frac{a \cdot L_1^2 \cdot (F_2 - F_1)}{16 \cdot (w_2 - w_1)} \tag{1}$$

$$EI_t = \frac{3 \cdot a \cdot L^2 - 4 \cdot a^3}{24 \cdot \left(2 \cdot \frac{w_2 - w_1}{F_2 - F_1}\right)} \tag{2}$$

In such expressions, L is the span; $L1$ is the reference distance for the analysis of the central area without shear stress; a is the distance between a loading position and the nearest support, (F_2–F_1) is the increment of load on the regression line with a correlation coefficient of 0.99 or better; and (w_2-w_1) is the increment of deflection in the same range.

As these were large-scale pieces, an experimental campaign was designed in such a way as to allow inspection by means of DIC at the end and centre of the pieces, and the reuse of the specimens in other types of tests, optimizing the investment of resources. In this sense, it was decided not to break a specimen of each length in order to reuse them in long-term tests under permanent load and changing hygrothermal conditions. Likewise, in order to take advantage of the ends of the pieces tested in a later test as cantilever beams, it was considered appropriate, once the service load had been largely exceeded, to limit the maximum load applied to another of the specimens of each length. This was done with the aim of preventing the failure of the pieces during the four-point bending test from damaging the ends of the pieces.

Consequently, three types of tests were performed:

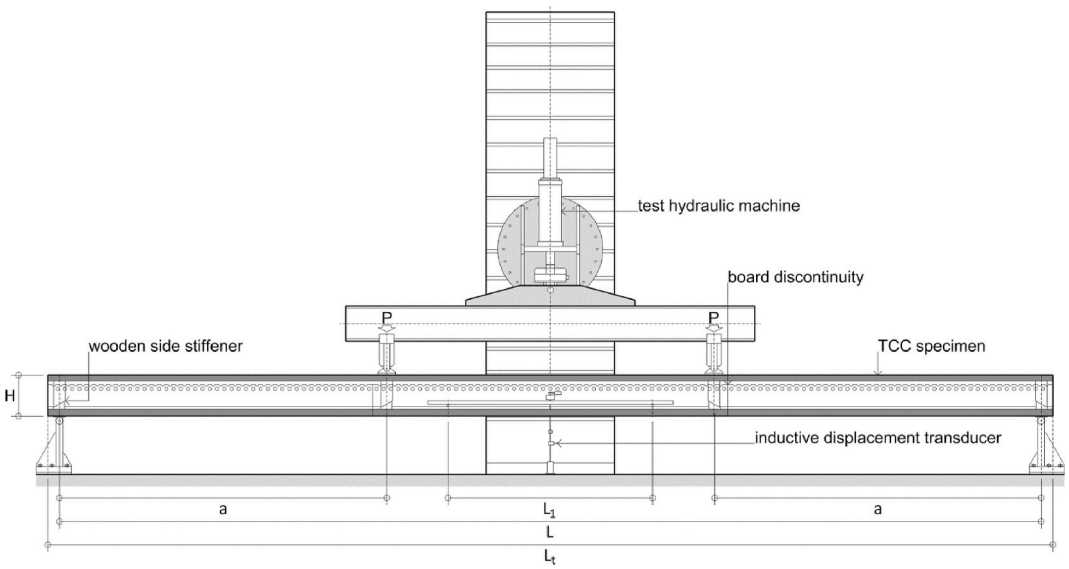

Fig. 4. Bending test instrumentation.

Fig. 5. Test setup.

A) Test until the service load is reached (F_{SLS}). To determine this load value, a permanent uniformly distributed load of 2.0 kN/m^2 of the structure's self-weight and 2.0 kN/m^2 of finishes, and a variable load of 5.0 kN/m^2 have been considered. Likewise, it was decided to consider the total load (9.0 kN/m^2), without discounting the self-weight of the piece, in order to measure the deformations of the element under the total design load. Since the test is carried out by means of two concentrated forces, applied in the thirds of the span, for the purposes of bearing capacity, an equivalent P loads were considered producing the same maximum bending, in accordance with expression (3):

$$P = \frac{3 \cdot q \cdot L}{8} \tag{3}$$

Consequently, and taking into account that the specimens have a width of 60 cm, the total forces ($F=2P$), corresponding to the total service load of each of the span tested, are 24.30, 29.16 and 34.02 kN, for 6.00, 7.20 and 8.40 m span, respectively. However, the first test (250.1-A) was completed by applying 18.85 kN, a value corresponding to a distributed load of 7 kN/m^2 (2.0 self-weight, 2.0 finishes, and 3.0 imposed). After this first contrast test, and in view of the good behaviour observed, it was decided to increase the service load in the tests An up to 9.0 kN/m^2 already mentioned.

B) Test up to a limit value (FLIM) that was analytically estimated so that the maximum stresses in the wood did not exceed 90% of the characteristic value of its resistance to bending, which led to values of 110 and 130 kN for the 7.20 and 8.40 m span. These load values correspond to equivalent surface loads of 33.95 kN/m^2 and 34.39 kN/m^2, for the indicated spans. This criterion of limiting the value of the load was decided as a result of the incident that occurred in the test of specimen 250.2. Upon reaching a load value of 84.23 kN, an intense breaking sound was heard. The test was then stopped and the specimen unloaded. However, a detailed visual inspection did not identify any cracking. Consequently, the test was restarted, reaching a value of 100 kN in this second load cycle. As will be seen in the following section, the failure of specimens 250.1 and 250.2 produced longitudinal cracks affecting the entire specimen, and invalidating it for its subsequent reuse in the end tests as cantilever beams.
C) Test until reaching the breaking load (F_{ULS}).

The Aramis 3D sensor was placed in the central area in type A tests, and in one of the extreme supports in types B and C.

4. Results and discussion

4.1. Load capacity and failure modes

Table 3 collects the results of the 15 tests carried out, including the maximum load (F) applied in each test. The F_{ULS} values correspond to the four prolonged tests until failure. The most unfavourable case corresponds to specimen 250.2-B, with an ultimate load of 100.0 kN. Adding the self-weight of the specimen (1.2 kN/m) supposes a total equivalent load of 39.04 kN/m^2, 4.3 times higher than the serviceability limit state for areas of public use (9.0 kN/m^2, broken down into 2.0 of self-weight, 2.0 of finishes, and 5.0

Table 3
Test results.

Specimen		Geometric parameters				Applied loads			Estimation of deflections in service situation										Stiffness		
		H	L	a	L_1	F_{SLS}	F_{LIM}	F_{ULS}	F_3	w_3	w_{3L1}	F_5	w_5		F_9	w_9		w_{9L1}	$EI_{t,L1}$	EI_t	RSD_{EI}
		mm	mm	mm	mm	kN	kN	kN	kN	mm	mm	kN	mm		kN	mm		mm	kN·m^2	kN·m^2	%
250.1	A	250	6000	2000	1250	18.85			7.92	2.70	0.08	13.21	4.48	L/1340							
	C							150.40		2.69	0.10		4.49	L/1335	23.77	8.46	L/709	0.35	12375	10517	5.62
250.2	A					24.29				2.94	0.09		4.99	L/1202		9.34	L/642	0.34			
	B							100.00		3.02	0.08		5.14	L/1168		9.50	L/632	0.32	12619	9376	
250.3	A					24.31				2.68	0.09		4.90	L/1224		9.18	L/653	0.33	12834	9336	
300.1	A	300	7200	2400	1500	29.21			9.51	3.85	0.10	15.85	6.50	L/1107	28.53	11.91	L/605	0.44			
	C							145.09		3.82	0.12		6.48	L/1111		11.82	L/609	0.46	18889	15752	5.42
300.2	A					29.21				3.66	0.14		6.32	L/1139		12.00	L/600	0.47			
	B						110.01			3.57	0.08		6.01	L/1197		11.09	L/649	0.38	21122	16740	
300.3	A					29.21				3.80	0.13		6.59	L/1092		12.40	L/581	0.45	19927	14654	
350.1	A	350	8400	2800	1750	33.96			11.09	4.50	0.08	18.49	7.59	L/1107	33.28	13.98	L/601	0.41			
	C							166.18		4.41	0.14		7.46	L/1126		13.75	L/611	0.46	36318	25005	4.60
350.2	A					33.98				4.63	0.16		7.86	L/1069		14.54	L/578	0.52			
	B						130.00			4.31	0.08		7.21	L/1165		13.38	L/628	0.42	35204	25730	
350.3	A					34.00				4.54	0.13		7.85	L/1070		14.66	L/573	0.50	32322	23050	

imposed in category C5), and 7.8 times that of floors for residential use with partitions and light finishes (5.0 kN/m^2).

In type C tests, the central extensometer is removed at an intermediate stage to avoid damage. In these cases, the measurement of deformations was completed with the stroke of the load application head.

In all the tests carried out until failure, it occurs abruptly, although preceded by characteristic sounds of fibre breakage, and with a large curvature of the piece (Fig. 6). The failure begins in the glulam flange, upon reaching its tensile bearing capacity in the area subjected to the maximum bending moment. The critical section seems to be conditioned by the presence of some kind of discontinuity, like knots or finger joints (Fig. 7). In any case, once the failure has started, longitudinal cracks occur and detachment of the plywood rib, which extends to the ends of the piece (Fig. 8). Under these conditions, the concrete slab, which previously had not shown any damage, also begins to crack, with the classic bending pattern (Fig. 9).

4.2. Bending stiffness and composite action

Fig. 10 shows the load-displacement curves obtained for each of the three spans tested. In type B tests, from a certain load value, the extensometers were also removed to avoid damage. Then, the curves were completed with the information obtained by DIC, and processed with the Gom Correlate software (Zeiss®). As indicated, in the case of the tests carried out until failure (type C), the graphs have been completed with the measurement of the load head stroke. The loads corresponding to the serviceability limit state indicated in figure (24.30, 29.16 and 34.02 kN) correspond to a total distributed load of 9.0 kN/m^2, as previously determined.

For the bending stiffness analysis, the equivalence between point load test actions (P') and uniformly distributed service actions (q) is carried out considering the equality of deflection. This consideration leads to the equation:

$$P' = \frac{135 \cdot q \cdot L}{368} \tag{4}$$

Table 3 shows the deflections corresponding to different load levels in a service situation: 9 kN/m^2 (*F9*), associated with a category C5 (public access), 5 kN/m^2 (*F5*), relative to a category A (residential) with light finishes, and finally 3 kN/m^2 (*F3*). The two extreme situations define the load steps to apply equations (1) and (2) to determine the bending stiffness in local (relative to L_1) and global (relative to L) terms.

Throughout the entire loading process, a substantially linear and homogeneous behaviour is observed. Within each set, this uniformity is also deduced from the comparison of the stiffness values EI_t obtained with equation (2). Its relative standard deviation (RSD_{EI}) is between 4.60 and 5.62%. It can be seen how the global stiffness of the samples experiences a reduction with respect to the local stiffness measured in the centre of the specimen. This reduction is 22.7%, 21.3% and 28.9% for the tests with 250, 300 and 350 mm depths, respectively, and is due to the influence of the shear force on the stiffness of the assembly.

The relative deflection values are between L/1069 and L/1340 for 5 kN/m^2, and between L/573 and L/709 for 9 kN/m^2. Despite the slenderness of the samples (L/24), the results largely satisfy the requirement usually associated with the assessment of integrity of the construction elements and user comfort. And all of this regardless of the fact that the system developed allows applying precambers and making semi-rigid and continuous joints, which would result in an even much more favourable behaviour than that described.

The stiffness deduced by the tests has also been compared with the two most widely used estimation criteria in the technical

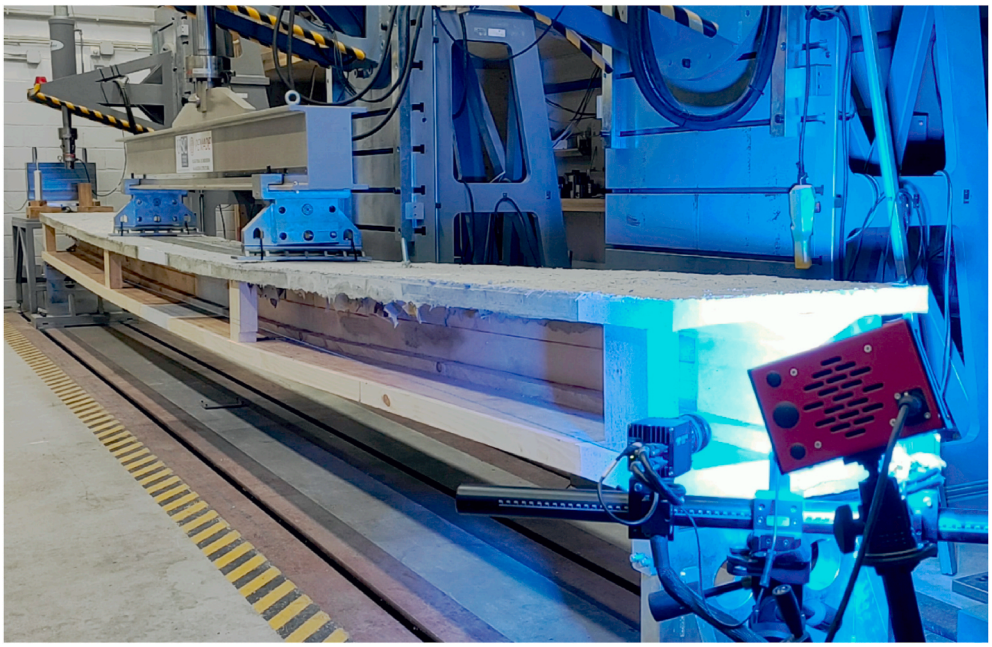

Fig. 6. Image of the 350.1-C test at the instant prior to rupture (capture extracted from video).

Fig. 7. Photographs of the underside of the glulam flange at the end of tests 250.2-B and 300.1-C. On the left, a break initiated in a finger joint (near one of the plywood rib discontinuities) can be seen.

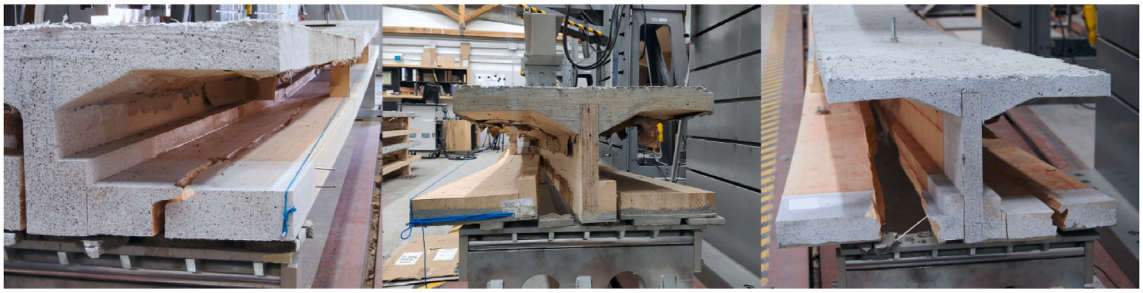

Fig. 8. Longitudinal failures of the glulam flange in tests 250.2-B, 300.1-C, and 350.1-C.

Fig. 9. Cracking in the concrete slab. Test 350.1-C.

literature for TCC elements. First, the Gamma Method, outlined in Eurocode 5, Part 1.1 - Annex B [65], has been used. This simplified procedure assumes that the system is composed of wood and concrete fractions, subjected to Euler-Bernoulli bending, and linked by connections with a certain degree of flexibility. It thus leads to an effective bending stiffness that depends on the geometry of the cross section and the properties of the materials, according to the expression:

$$EI_{eff,\gamma} = \sum_i \left(E_i \cdot I_i + \gamma \cdot E_i \cdot A_i \cdot a_i^2\right) \tag{5}$$

The subscript i refers to the different layers of timber or concrete, in each one being E its elastic modulus, I the moment of inertia, A the cross-sectional area, and a_i the distance between its centroid and the effective neutral axis of the composite section. The γ parameter, which gives the method its name, is defined in the range 0 (no composite action) to 1 (full composite action) using the expression:

$$\gamma = \frac{1}{1 + \frac{\pi^2 \cdot E \cdot A}{K_s \cdot L^2}} \tag{6}$$

L is the length of the span, and K_s is the slip modulus of the connection. The last data has been deduced from the previous test

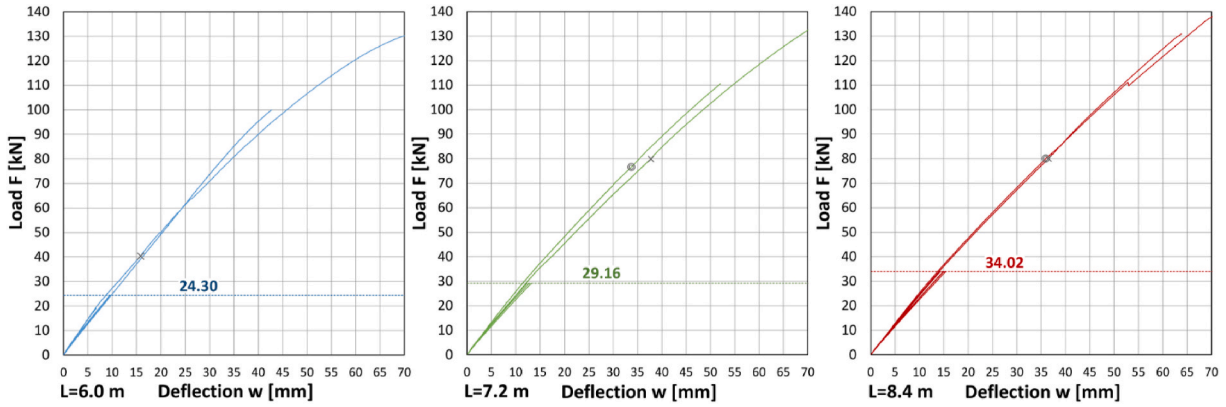

Fig. 10. Load-deflection curves. In each case, the estimated F_{SLS} service load has been indicated. Circles and crosses indicate the moment in which the extensometers are removed, and the displacement measurement is completed by means of DIC or loading equipment, respectively.

campaign, carried out with samples of a single plywood rib (series B2R) [56,57].

The alternative procedure is the one developed by U.A. Girhammar [66,67], based on the values of bending stiffness of the non-composite section ($EI_{0\%}$) and fully composite section ($EI_{100\%}$)

$$EI_{eff,G} = EI_{\infty}\left[1 + \frac{EI_{\infty}/EI_0 - 1}{1 + (\mu/\pi)^2 \cdot (\alpha \cdot L)^2}\right]^{-1} \tag{7}$$

In the previous expression, the parameter α depends again on the slip modulus of the connection, and on the distance *r* between the centroids of the connected parts.

$$\alpha = \sqrt{\frac{K \cdot r^2}{EI_0 \cdot (1 - EI_0/EI_{\infty})}} \tag{8}$$

Table 4 shows the effective bending stiffness values for each of the tested specimens, estimated by both procedures, and considering the slip modulus with both its average value and its 5th percentile value. Analogously, the values thus obtained have been compared with the results of the experimental campaign. It is observed that the Girhammar formulation achieves a better fit in all cases, both in average and characteristic values, even though in the latter it can lead, for the longest specimens, to an overestimation of less than 0.4%. This conclusion is also illustrated through Fig. 11, which shows a comparison between the load-displacement graphs obtained with the average bending stiffness of the tests and the effective values deduced with both formulations from the average slip modulus.

In any case, the previous experimental adjustment of the slip modulus is considered essential, for example, by performing the push-out shear test as defined in the EN 26891:1991 standard [68].

On the other hand, it should be noted that the maximum displacements turn out to be between 6.8 and 13.0 times those corresponding to the estimated service load for a building for public use (9 kN/m^2). Even when the curves do not present areas of plastic behaviour, it can be established that the deformations produced between SLS and ULS guarantee a global ductility suitable for the intended uses.

Table 4 also includes a column that establishes the relationship between the bending stiffness obtained in each test (EI_t) and that which would correspond to a full composite action ($EI_{100\%}$). It is observed that the first is between 76.04% and 91.39% of the second, with an average of 83.16%. The only external sign of slippage occurred in test 250.1-C, in a state very close to failure. Some slippage can be observed in the plywood, roughly coinciding with the bottom of the internal holes (Fig. 12). On the contrary, in the remaining cases a mere rotation of the extreme section around the support is observed, without any evidence of sliding between materials (Fig. 13).

The deformational behaviour of the representative sections has also been analysed by means of DIC. Fig. 14 shows the tracking points and inspection labels corresponding to the central area of specimen 350.2-B in two stages of the loading process. Fig. 15 shows the distribution of strains in the analysed points of the central section for different load values. It can be seen that the resulting position of the neutral axis is approximately at the height of the centroid of the section, and at the lower limit of the concrete. In this way, the latter assumes almost all of the compression stresses, while the timber fraction supports the tensile ones. This achieves an effective use of the materials involved in the composite solution.

The results indicate that the proposed connection is very suitable in terms of strength, stiffness, and composite action, with limited use of adhesives or steel.

4.3. Vibration serviceability

European regulations [69] include the effects of vibrations in serviceability limit state to avoid discomfort to users and damage to construction elements. To do this, the document states that the natural frequency should be kept above appropriate values which

Table 4
Bending stiffness analysis.

Specimen		$EI_{0\%}$	$EI_{100\%}$	$EI_{t,L1}$	EI_t	$EI_t/EI_{100\%}$	$EI_{t,L1,ave}$	$EI_{t,ave}$	$EI_{t,5th}$	Estimation with $K_{s,ave}$ 283537 kN/m				Estimation with $K_{s,5th}$ 236534 kN/m			
										$EI_{eff,\gamma}$	$EI_{eff,\gamma}/EI_{t,ave}$	$EI_{eff,G}$	$EI_{eff,G}/EI_{t,ave}$	$EI_{eff,\gamma}$	$EI_{eff,\gamma}/EI_{t,5th}$	$EI_{eff,G}$	$EI_{eff,G}/EI_{t,5th}$
		kN·m²	kN·m²	kN·m²	kN·m²	%	kN·m²	kN·m²	kN·m²	kN·m²	%	kN·m²	%	kN·m²	%	kN·m²	%
250.1	C	692.9	12165.7	12375.3	10517.3	86.45	12609.4	9743.2	9340.0	8277.2	84.95	9054.3	92.93	7807.8	83.60	8626.8	92.36
250.2	B			12618.7	9376.5	77.07											
250.3	A			12834.3	9335.9	76.74											
300.1	C	972.9	19271.2	18889.4	15752.3	81.74	19979.5	15715.5	14763.8	14497.5	92.25	15392.4	97.94	13843.7	93.77	14809.6	100.31
300.2	B			21121.9	16740.2	86.87											
300.3	A			19927.1	14654.0	76.04											
350.1	C	1378.3	28154.3	36318.4	25004.7	88.81	34614.7	24594.8	23245.2	22659.4	92.13	23585.9	95.90	21841.0	93.96	22857.7	98.33
350.2	B			35204.0	25730.0	91.39											
350.3	A			32321.7	23049.7	81.87											

$EI_{0\%}$ *Cross-sectional stiffness considering that there is no composite action at all.*
$EI_{100\%}$ *Cross-sectional stiffness considering full composite action.*
$EI_{t,L1}$ *Local stiffness obtained by expression (1) from the test results.*
EI_t *Global stiffness obtained by expression (2) from the test results.*
$EI_{eff,\gamma}$ *Effective stiffness obtained by the Gamma Method.*
$EI_{eff,G}$ *Effective stiffness obtained by the Girhammar procedure.*
The subscripts ave and 5th *indicate, respectively, average values and* 5th *percentile characteristic values.*

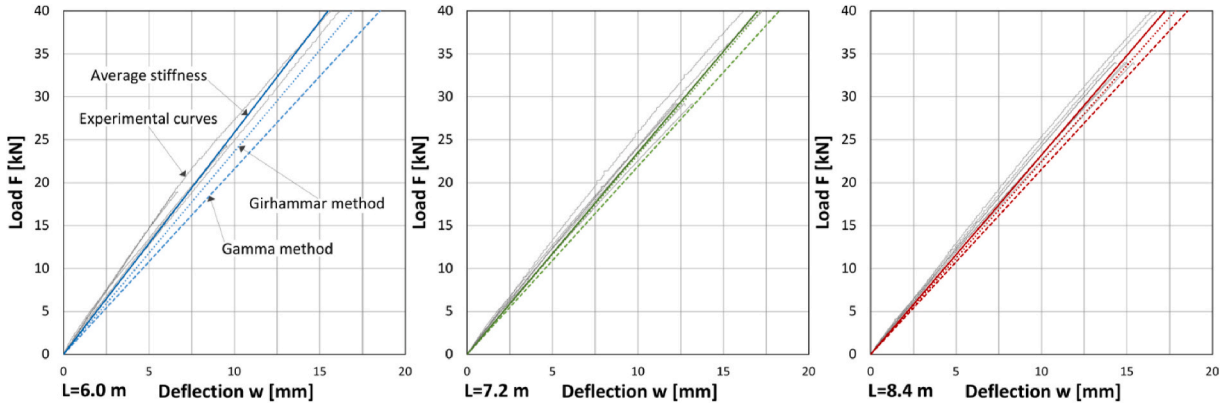

Fig. 11. Comparison of load-displacement curves obtained with the different bending stiffnesses: average (continuous line), gamma method (dotted line), and Girhammar method (dashed line).

Fig. 12. Slippage of the connection in the 250.1-C test.

Fig. 13. End section in the 300.1-C test.

depend upon the use of the building and the source of the vibration. In this sense, and specifically in relation to wooden residential floors, Eurocode 5 [65] only recommends adopting 8 Hz as a reference value, below which a special investigation should be made. In order to relate the vibration effects with the comfort assessment, the criteria of two references linked to the process of updating European regulations have been taken into account: the one developed by the SC5/WG3/subgroup 4 team [70], in relation to the Eurocode 5, and the technical report EUR 24084 EN [71], within the framework of the CEN/TC 250 program.

The first document defines vibration criteria through six floor performance levels, for which no further investigations are necessary if the requirements from Table 5 are satisfied. In addition, Table 6 contains recommendations for level selection based on the use

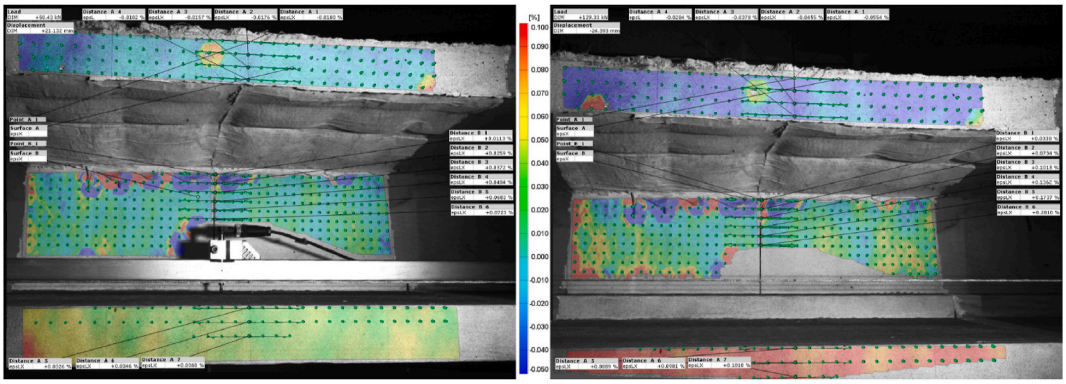

Fig. 14. DIC analysis of specimen 350.2-B at steps 15 and 45 (total number of stages until equipment removal: 63).

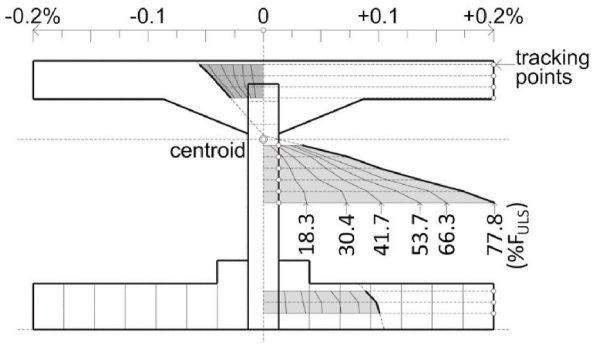

Fig. 15. Strain distributions of the central section of specimen 350.2-D obtained by DIC for different load values.

category and possible choices related to economy and construction quality criteria. For resonant vibration design situations ($f_1 < 8$ Hz), the minimum fundamental frequency, acceleration and stiffness criteria should be fulfilled, and for transient vibration design situations ($f_1 \geq 8$ Hz) only velocity and stiffness criteria are required. The value of f_1 can be obtained according to equation (9).

$$f_1 = \frac{\pi}{2} \cdot \sqrt{\frac{EI_y}{\mu \cdot L^4}} \cdot \sqrt{1 + \left[2 \cdot \left(\frac{b}{L}\right)^2 + \left(\frac{b}{L}\right)^4\right] \cdot \frac{EI_x}{EI_y}} \tag{9}$$

where μ is the mass per square meter (kg/m^2); L is the span of the floor (m) (in x-direction); b is the width of the floor (m) (in y-direction); EI_x is the stiffness (N·m^2) about the x-axis; and EI_y is the stiffness (N·m^2) about the y-axis. The method associates the mass to the quasi-permanent fraction of the imposed loads, limiting those derived from use to 10% of their characteristic values. For the estimation of EI_x, only the upper concrete slab, 50 mm thick, has been considered. Regarding EI_y, the technical report establishes that the initial elastic stiffness should be used, including a dynamic modulus of elasticity for concrete 10% larger than the static tangent modulus (E_{cm}).

The problem at this point is precisely establishing the initial elastic stiffness. The values in Table 4 correspond to the four-point bending test, estimated either for the central area not subjected to shear, or for the whole piece. However, in a service situation, the global stiffness must take a value between the two. For its determination, specimens 250.3-A, 300.3-A and 350.3-A were subjected to a specific test. The procedure consisted of exciting the system by an impulse reached by hitting with an instrumented hammer, and measuring the response with a Bosch Sensortec BMI160 inertial measurement unit. The deduced frequencies were, respectively, 12.0, 11.2 and 10.9 Hz (Fig. 16), and the bending stiffness was calculated according to equation (10) included in Eurocode 5:

$$f_{hit} = \frac{\pi}{2 \cdot L^2} \cdot \sqrt{\frac{EI}{\mu}} \quad \rightarrow \quad EI = \mu \cdot \left(\frac{2 \cdot L^2 \cdot f_{hit}}{\pi}\right)^2 \tag{10}$$

The resulting stiffnesses for the three spans analysed (9972.2, 19194.6 and 29176.4 kN m^2) are consistent with the previous considerations and the different test conditions.

Table 7 collects the frequency values in the service situation, obtained for the six cases resulting from the combination of spans and uses. It is observed that all of them correspond to transient vibration design situations, with the only exception of the last one, associated with the maximum span and load.

Table 5
Floor vibration criteria according to floor performance level [64].

	Floor performance levels						
Criteria	I	II	III	IV	V	VI	VII
Stiffness criteria for all floors w_{1kN} [mm] ≤	0.25	0.25	0.5	0.8	1.2	1.6	no criteria
Response factor R ≤	4	8	12	16	24	32	
Frequency criteria for all floors f_1 [Hz] ≥	4.5						
Acceleration criteria for resonant vibration design situations a_{rms} [m/s^2] ≤	R x 0.005						
Velocity criteria for transient vibration design situations v_{rms} [m/s] ≤	R x 0.0001						

Table 6
Recommended selection of floor performance levels [64].

Use category		Quality choice	Base choice	Economy choice
A (residential)	Multi-storey	level I, II, III	level IV	level V
	Single house	level I, II, III, IV	level V	level VI
B (office)		level I, II	level III	level IV

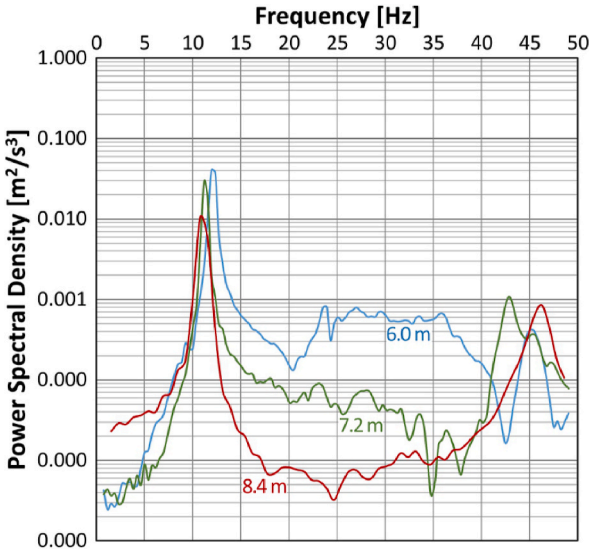

Fig. 16. Curves PSD-Frequency.

The stiffness criteria, applicable in all cases, involves determining the maximum deflection in the mid-span of a single span floor according to equation (11):

$$w_{1kN} = \frac{F \cdot L^3}{48 \cdot EI_y \cdot b_{ef}} \quad ; \quad b_{ef} = \min \begin{cases} \dfrac{L}{1.1} \cdot \sqrt[4]{\dfrac{EI_x}{EI_y}} \\ b \end{cases} \tag{11}$$

For transient vibration design situations, the velocity criteria should be fulfilled in addition. To do this, the root mean square velocity (m/s) must be calculated according to equation (12):

Table 7
Vibration serviceability parameters.

Case			mass	bending stiffness			stiffness criteria		velocity criteria									acceleration criteria	
	b	L	μ	EI_x	EI_y	f_1	b_{ef}	w_{1kN}	ξ	K_{imp}	η	β	I_m	m	M*	V_{rms}	R	a_{rms}	R
	m	m	kg/m	N·m^2	N·m^2	Hz	m	mm	%				N·s	kg/m^2	kg	mm/s		mm/s^2	
250.Q5	0.6	6.0	195.7	424174.1	9929567.3	9.83	0.60	0.45	2.50	1.00	0.97	0.51	3.84	305.81	550.46	0.25	2.52		
250.Q9			275.2			8.29	0.60	0.45	2.50	1.00	0.97	0.52	4.80	407.75	733.94	0.24	2.42		
300.Q5	0.6	7.2	195.7	424174.1	19580193.1	9.59	0.60	0.40	2.50	1.00	0.97	0.51	3.97	305.81	660.55	0.22	2.18		
300.Q9			275.2			8.08	0.60	0.40	2.50	1.00	0.97	0.52	4.96	407.75	880.73	0.21	2.10		
350.Q5	0.6	8.4	195.7	424174.1	29792138.1	8.69	0.60	0.41	2.50	1.00	0.97	0.52	4.51	305.81	770.64	0.22	2.16		
350.Q9			275.2			7.32	0.60	0.41	2.50	1.00	0.97	0.53	5.63	407.75	1027.52	0.21		20.98	4.20

$$\begin{cases} V_{rms} = \beta \cdot K_{imp} \cdot K_{red} \cdot \dfrac{I_m}{M^*} \\ R = \dfrac{V_{rms}}{0.0001} \end{cases} \quad \begin{cases} K_{imp} = \max \begin{cases} 0.48 \cdot \left(\dfrac{b}{L}\right) \cdot \left(\dfrac{EI_y}{EI_x}\right)^{0.25} \\ 1.0 \end{cases} \\ \eta = \begin{cases} 1.52 - 0.55 \cdot K_{imp} \;\; when \;\; 1.0 \le K_{imp} \le 1.5 \\ 0.69 \;\; else \end{cases} \\ \beta = (0.65 - 0.01 \cdot f_1) \cdot (1.22 - 11.0 \cdot \zeta) \cdot \eta \\ I_m = \dfrac{42 \cdot f_w^{1.43}}{f_1^{1.3}} \\ M^* = \dfrac{m \cdot L \cdot b}{2} \end{cases} \tag{12}$$

where K_{imp} is the impulsive multiplier factor; K_{red} is a reduction factor (0.7), taking into account that the exciting source on the floor and the sensing person are at a distance from each other; I_m is the mean modal impulse (N·s); f_w is the walking frequency (1.5 Hz); M^* is the floor modal mass (kg); and m is the floor self-weight per area (kg/m^2). In the previous expressions, a modal damping ratio (ζ) of value 0.025 has been adopted in accordance with reference [70] for timber-concrete floors.

On the other hand, with resonant vibration design situations, acceleration criteria must be considered, using the root mean square acceleration (m/s^2) according to equation (13):

$$\begin{cases} a_{rms} = \dfrac{0.4 \cdot \alpha \cdot F_0}{\sqrt{2} \cdot 2 \cdot \zeta \cdot M^*} \\ R = \dfrac{a_{rms}}{0.005} \end{cases} \tag{13}$$

where α is the Fourier coefficient depending on the fundamental frequency ($\alpha = e^{-0.4 \cdot f1}$); and F_0 is the vertical load of a walking person (usually taken as 700 N).

All associated parameters have also been compiled in Table 7. All cases show an eigenfrequency value higher than 8.0 Hz (transient vibration design situations), with the only exception of the longest span and load combination, which shows 7.32 Hz (resonant vibration design situation). The first ones have a response factor between 2.10 and 2.52 according to the velocity criterion, well below the limit (4) corresponding to a floor performance level I. In the only case with resonant behaviour, the factor obtained by the acceleration criterion increases to 4.2, which corresponds to a level II. Based on the stiffness criterion, the estimated maximum deflection values are between 0.40 and 0.45 in all cases, which is associated with a level III. This performance level is considered adequate for single houses and multi-storey buildings with a quality choice, and for office buildings with a base choice. As a result, the vibration behaviour of the TCC floor can be considered very favourable. In addition, it should be noted that the system allows semi-rigid and continuous connections to be made, which would produce a notable improvement in performance not included in the analysis.

5. Conclusions

The flexural behaviour of a new TCC flooring system has been experimentally analysed using full scale tests. The prototypes featured a double T configuration. The central plywood rib was glued together with the lower glulam flange, forming a prefabricated inverted T. On the other hand, the connection between the rib and the upper concrete slab, cast in place, was resolved by penetrating the concrete in the holes made in the upper part of the rib. A reduced number of transverse corrugated steel bars were added to make the joint more ductile. This connection reduces the consumption of adhesives and metal compared to other alternatives, proposing a composite in which it is intended to adapt the use of each material to its main benefits and achieve an eco-friendlier solution. On the other hand, the system has a self-weight of less than 1.2 kN/m (2.0 kN/m^2), which is very competitive compared to the usual only concrete solutions.

9 samples with a span of 6.0, 7.2 and 8.4 m, and a slenderness ratio of L/24, were subjected to a four-point bending test. The samples tested until failure showed a load capacity not less than 7.8 times the estimated one in residential buildings (5.0 kN/m^2), with deflections between L/1069 and L/1340, and 4.3 times that relative to buildings for public use (9.0 kN/m^2), with deflections between L/573 and L/709. The results indicate that the proposed system is adequate, both in SLS and in ULS. Additionally, between both states there is a notable increase in deformation, which constitutes a globally ductile response, as is always desirable in the field of building structures.

Additionally, the effective bending stiffness has been analysed by comparing the experimental results with the estimates of the Gamma Method and the formulation proposed by Girhammar. The latter achieves a better approximation, in any case starting from a previous experimental determination of the slip modulus of the connection used. The proposed connection presents satisfactory behaviour in terms of strength, stiffness and composite action (77.62–97.12%), all with a very simple construction process and a certain economy in the consumption of materials.

The behaviour before vibrations in service limit state has also been analysed in relation to comfort assessment. Three span lengths (6.0, 7.2 and 8.4 m) and two possible loading situations (5.0 kN/m^2 for residential and 9.0 kN/m^2 for public use) have been considered. All combinations show transient behaviour ($f_1 \geq 8$ Hz), with the only exception with the highest span and load. In any case, the most restrictive vibration analysis criteria lead to a performance level III. This level is considered to be adequate from the point of view of ensuring comfort for single houses and multi-storey levels with a quality choice and for office buildings with a base choice.

Future tests are necessary to verify the behaviour of these floors in continuity, incorporating corrugated steel bars in the concrete slab to withstand negative bending moments on the supports. Likewise, its long-term behaviour must be contrasted by means of specific tests.

Declaration of competing interest

The authors declare that they have no known competing financial interests or personal relationships that could have appeared to influence the work reported in this paper.

Data availability

Data will be made available on request.

Acknowledgements

This study is part of the research project “High-performance timber-concrete-composite hollow-core floors for sustainable and eco-efficient construction (AlveoTCC, with reference PID2019-107859RB-I00)”. The study developed was financed by the Spanish Ministry of Science and Innovation.

References

[1] United Nations Environment Programme, Global status report for buildings and construction. Towards a zero-emissions, in: efficient and resilient buildings and construction sector, 2021. Nairobi, http://globalabc.org/resources/publications.
[2] International Energy Agency, Energy Efficiency 2021, OECD Publishing, Paris, 2021, https://doi.org/10.1787/cfb80e1e-en.
[3] M. Röck, M.R. Mendes, M. Balouktsi, F. Nygaard, H. Birgisdottir, R. Frischknecht, G. Habert, T. d, Life cycle assessment framework for the optimisation of facades and fenestration in building envelopes, J. Build. Eng. 43 (2021), 103138, https://doi.org/10.1016/j.jobe.2021.103138.
[8] M.K. Nematchoua, M. Sadeghi, S. Reiter, Strategies and scenarios to reduce energy consumption and CO_2 emission in the urban, rural and sustainable neighbourhoods. Sustainable CitieLützkendorf, A. Passer, in: Embodied GHG emissions of buildings - The hidden challenge for effective climate change mitigation. Applied Energy, 258, 2020, 114107, https://doi.org/10.1016/j.apenergy.2019.114107.
[4] Y. Dong, S.T. Ng, P. Liu, A comprehensive analysis towards benchmarking of life cycle assessment of buildings based on systematic review, Build. Environ. 204 (2021), 108162, https://doi.org/10.1016/j.buildenv.2021.108162.
[5] X.J. Luo, L.O. Oyedele, Assessment and optimisation of life cycle environment, economy and energy for building retrofitting, Energy Sustain. Develope. 65 (2021) 77–100, https://doi.org/10.1016/j.esd.2021.10.002.
[6] T. Joensuu, R. Leino, J. Heinonen, A. Saari, Developing buildings’ life cycle assessment in circular economy-comparing methods for assessing carbon footprint of reusable components, Sustain. Cities Soc. 77 (2022), 103499, https://doi.org/10.1016/j.scs.2021.103499.
[7] A. Feehan, H. Nagpal, A. Marvuglia, J. Gallagher, Adopting an integrated building energy simulation an, Society 72 (2021), 103053, https://doi.org/10.1016/j.scs.2021.103053.
[9] I. Zabalza, A. Valero, A. Aranda, Life cycle assessment of building materials: comparative analysis of energy and environmental impacts and evaluation of the eco-efficiency improvement potential, Build. Environ. 46 (5) (2011) 1133–1140, https://doi.org/10.1016/j.buildenv.2010.12.002.
[10] J. Hansted, N. Lin, M. Walbech, Comparative life cycle assessment of cross laminated timber building and concrete building with special focus on biogenic carbon, Energy Build. 254 (2022), 111604, https://doi.org/10.1016/j.enbuild.2021.111604.
[11] Organisation for Economic Cooperation and Development, Global Material Resources Outlook to 2060: Economic Drivers and Environmental Consequences, OECD Publishing, Paris, 2019, https://doi.org/10.1787/9789264307452-en.
[12] A. Stocchero, J.K. Seadon, R. Falshaw, M. Edwards, Urban Equilibrium for sustainable cities and the contribution of timber buildings to balance urban carbon emissions: a New Zealand case study, J. Clean. Prod. 143 (2017) 1001–1010, https://doi.org/10.1016/j.jclepro.2016.12.020.
[13] M. Caniato, A. Marzi, S. Monteiro, A. Gasparella, A review of the thermal and acoustic properties of materials for timber building construction, J. Build. Eng. 43 (2021), 103066, https://doi.org/10.1016/j.jobe.2021.103066.
[14] M. Bazli, M. Heitzmann, H. Ashrafi, Long-span timber flooring systems: a systematic review from structural performance and design considerations to constructability and sustainability aspects, J. Build. Eng. 48 (2022), 103981, https://doi.org/10.1016/j.jobe.2021.103981.
[15] A. Trummer, S. Krestel, S. Aicher, KIELSTEG - defining the design parameters for a lightweight wooden product, in: WCTE 2016 - World Conference on Timber Engineering, Technische Universität Wien, 2016.
[16] D.L. Achat, M. Fortin, G. Landmann, B. Ringeval, L. Augusto, Forest soil carbon is threatened by intensive biomass harvesting, Sci. Rep. 5 (2015), 15991, https://doi.org/10.1038/srep15991.
[17] A. Ahmad, Q. Liu, S.M. Nizami, A. Mannan, S. Saeed, Carbon emission from deforestation, forest degradation and wood harvest in the temperate region of Hindukush Himalaya, Pakistan between 1994 and 2016, Land Use Pol. 78 (2018) 781–790, https://doi.org/10.1016/j.landusepol.2018.07.009.
[18] A. Ceccotti, Composite concrete-timber structures, Prog. Struct. Eng. Mater. 4 (3) (2002) 264–275, https://doi.org/10.1002/pse.126.
[19] D. Yeoh, M. Fragiacomo, M. De Franceschi, K. Heng, State of the art on timber-concrete composite structures: literature review, J. Struct. Eng. 137 (10) (2011), https://doi.org/10.1061/(ASCE)ST.1943-541X.0000353.
[20] A. Siddika, A. Al Mamun, F. Aslani, Y. Zhuge, R. Alyousef, A. Hajimohammadi, Cross-laminated timber–concrete composite structural floor system: a state-of-the-art review, Eng. Fail. Anal. 130 (2021), 105766, https://doi.org/10.1016/j.engfailanal.2021.105766.
[21] S. Di Nino, A. Gregori, M. Fragiacomo, Experimental and numerical investigations on timber-concrete connections with inclined screws, Eng. Struct. 209 (2020), 109993, https://doi.org/10.1016/j.engstruct.2019.109993.
[22] H. Du, X. Hu, G. Han, D. Shi, Experimental and analytical investigation on flexural behaviour of glulam-concrete composite beams with interlayer, J. Build. Eng. 38 (2021), 102193, https://doi.org/10.1016/j.jobe.2021.102193.
[23] W.M. Sebastian, O.G.A. Bell, C. Martins, A.M.P.G. Dias, Experimental evidence for effective flexural-only stiffnesses to account for nonlinear flexural-slip behaviour of timber-concrete composite sections, Construct. Build. Mater. 149 (2017) 481–496, https://doi.org/10.1016/j.conbuildmat.2017.04.082.
[24] W. Zhu, H. Yang, W. Liu, B. Shi, Z. Ling, H. Tao, Experimental investigation on innovative connections for timber–concrete composite systems, Construct. Build. Mater. 207 (2019) 345–356, https://doi.org/10.1016/j.conbuildmat.2019.02.079.

[25] Z. Ling, H. Zhang, Q. Mu, Z. Xiang, L. Zhang, W. Zheng, Shear performance of assembled shear connectors for timber–concrete composite beams, Construct. Build. Mater. 329 (2022), 127158, https://doi.org/10.1016/j.conbuildmat.2022.127158.
[26] L. Zhang, Y. Hei, D. Tomlinson, Experimental investigation on the shear properties of notched connections in mass timber panel-concrete composite floors, Construct. Build. Mater. 234 (2020), 117375, https://doi.org/10.1016/j.conbuildmat.2019.117375.
[27] D. Otero-Chans, J. Estévez-Cimadevila, F. Suárez-Riestra, E. Martín-Gutiérrez, Experimental analysis of glued-in steel plates used as shear connectors in Timber-Concrete-Composites, Eng. Struct. 170 (2018) 1–10, https://doi.org/10.1016/j.engstruct.2018.05.062.
[28] J. Kanócz, V. Bajzecerová, Timber-concrete composite elements with various composite connections. Part 3: adhesive connection, Wood Res. 60 (6) (2015) 939–952.
[29] K. Quang, A. Park, K. Tan, K. Lee, Full-scale static and dynamic experiments of hybrid CLT–concrete composite floor, Construct. Build. Mater. 170 (2018) 55–65, https://doi.org/10.1016/j.conbuildmat.2018.03.042.
[30] S.A. Hadigheh, R. McDougall, C. Wiseman, L. Reid, Evaluation of composite action in cross laminated timber-concrete composite beams with CFRP reinforcing bar and plate connectors using Digital Image Correlation (DIC), Eng. Struct. 232 (2021), 111791, https://doi.org/10.1016/j.engstruct.2020.111791.
[31] N. Khorsandnia, H. Valipour, J. Schänzlin, K. Crews, Experimental investigations of deconstructable timber–concrete composite beams, J. Struct. Eng. 142 (12) (2016), 04046130, https://doi.org/10.1061/(ASCE)ST.1943-541X.0001607.
[32] L. Boccadoro, S. Zweidler, R. Steiger, A. Frangi, Bending tests on timber-concrete composite members made of beech laminated veneer lumber with notched connection, Eng. Struct. 132 (2017) 14–28, https://doi.org/10.1016/j.engstruct.2016.11.029.
[33] T. Tannert, A. Gerber, Till Vallee. Hybrid adhesively bonded timber-concrete-composite floors, Int. J. Adhesion Adhes. 97 (2020), 102490, https://doi.org/10.1016/j.ijadhadh.2019.102490.
[34] D. Denouwe, A. Messan, E. Fournely, A. Bouchaïr, Experimental study of the mechanical behavior of timber-concrete shear connections with threaded reinforcing bars, Eng. Struct. 172 (2018) 997–1010, https://doi.org/10.1016/j.engstruct.2018.06.084.
[35] J. Kanócz, V. Bajzecerová, S. Steller, Timber-concrete composite elements with various composite connections. Part 1: screwed connection, Wood Res. 58 (4) (2013) 555–570.
[36] J. Kanócz, V. Bajzecerová, S. Steller, Timber-concrete composite elements with various composite connections. Part 2: grooved connection, Wood Res. 59 (4) (2014) 627–638.
[37] D. Yeoh, M. Fragiacomo, B. Deam, Experimental behaviour of LVL-concrete composite floor beams at strength limit state, Eng. Struct. 33 (2011) 2697–2707, https://doi.org/10.1016/j.engstruct.2011.05.021.
[38] M. Fragiacomo, C. Amadio, L. MacOrini, Short- and long-term performance of the "Tecnaria'' stud connector for timber-concrete composite beams, Mater. Struct. 40 (2017) 1013–1026, https://doi.org/10.1617/s11527-006-9200-2.
[39] N. Naud, L. Sorelli, A. Salenikovich, S. Cuerrier-Auclair, Fostering GLULAM-UHPFRC composite structures for multi-storey buildings, Eng. Struct. 188 (2019) 406–4171, https://doi.org/10.1016/j.engstruct.2019.02.049.
[40] S. Lamothe, L. Sorelli, P. Blanchet, P. Galimard, Engineering ductile notch connections for composite floors made of laminated timber and high or ultra-high performance fiber reinforced concrete, Eng. Struct. 211 (2020), 110415, https://doi.org/10.1016/j.engstruct.2020.110415.
[41] T. Sartori, R. Crocetti, Prefabricated timber-concrete composite floors, Euro. J. Wood. Prod. 74 (2016) 483–485, https://doi.org/10.1007/s00107-016-1007-4.
[42] A. Hamid, Y. Hei, Stiffness prediction of mass timber panel-concrete, MTPC, Composite Connect Incline Screw Gap Eng. Struct. 207 (2020), 110215, https://doi.org/10.1016/j.engstruct.2020.110215.
[43] E. Appavuravther, B. Vandoren, J. Henriques, Behaviour of screw connections in timber-concrete composites using low strength lightweight concrete, Construct. Build. Mater. 286 (2021), 122973, https://doi.org/10.1016/j.conbuildmat.2021.122973.
[44] C. Martins, A.M.P.G. Dias, R. Costa, P. Santos, Environmentally friendly high performance timber–concrete panel, Construct. Build. Mater. 102 (2016) 1060–1069, https://doi.org/10.1016/j.conbuildmat.2015.07.194.
[45] G. He, L. Xie, X. Wang, J. Yi, L. Peng, Z. Chen, P.J. Gustafsson, R. Crocetti, Shear behavior study on timber-concrete composite structures with bolts, Bioresources 11 (4) (2016) 9205–9218, https://doi.org/10.15376/biores.11.4.9205-9218.
[46] J. Cao, H. Xiong, J. Chen, Mechanical performance of timber-concrete bolted connections under cyclic loading, Structures 34 (2021) 3464–3477, https://doi.org/10.1016/j.istruc.2021.09.086.
[47] B. Shi, W. Liu, H. Yang, Experimental investigation on the long-term behaviour of prefabricated timber-concrete composite beams with steel plate connections, Construct. Build. Mater. 266 (2021), 120892, https://doi.org/10.1016/j.conbuildmat.2020.120892 part A.
[48] K. Müller, A. Frangi, Micro-notches as a novel connection system for timber-concrete composite slabs, Eng. Struct. 245 (2021), 112688, https://doi.org/10.1016/j.engstruct.2021.112688.
[49] Ch Bedon, M. Fragiacomo, Three-dimensional modelling of notched connections for timber–concrete composite beams, Struct. Eng. Int. 27 (2) (2017) 184–196, https://doi.org/10.2749/101686617X14881932435295.
[50] Y. Jiang, X. Hu, W. Hong, J. Zhang, F. He, Experimental study of notched connectors for glulam-lightweight concrete composite beams, Bioresources 15 (2) (2020) 2171–2180, https://doi.org/10.15376/biores.15.2.2171-2180.
[51] S. Yilmaz, S. Demir, N. Vural, Experimental investigation of a prefabricated timber-concrete composite floor structure: notched-slab approach, Adv. Concrete Construct. 12 (1) (2021) 13–23, https://doi.org/10.12989/acc.2021.12.1.013.
[52] Q. Fu, L. Yan, T. Ning, B. Wang, B. Kasal, Behavior of adhesively bonded engineered wood – wood chip concrete composite decks: experimental and analytical studies, Construct. Build. Mater. 247 (2020), 118578, https://doi.org/10.1016/j.conbuildmat.2020.118578.
[53] J. Frohnmüller, J. Fischer, W. Seim, Full-scale testing of adhesively bonded timber-concrete composite beams, Mater. Struct. 54 (2021) 187, https://doi.org/10.1617/s11527-021-01766-y.
[54] B. Shan, Y. Xiao, W.L. Zhang, B. Liu, Mechanical behavior of connections for glubam-concrete composite beams, Construct. Build. Mater. 143 (2017) 158–168, https://doi.org/10.1016/j.conbuildmat.2017.03.136.
[55] J. Daňková, P. Mec, J. Šafrata, Experimental investigation and performance of timber-concrete composite floor structure with non-metallic connection system, Eng. Struct. 193 (2019) 207–218, https://doi.org/10.1016/j.engstruct.2019.05.004.
[56] J. Estévez-Cimadevila, E. Martín-Gutiérrez, F. Suárez-Riestra, D. Otero-Chans, J.A. Vázquez-Rodríguez, Timber-concrete composite structural flooring system, J. Build. Eng. 49 (2022), 104078, https://doi.org/10.1016/j.jobe.2022.104078.
[57] D. Otero-Chans, J. Estévez-Cimadevila, F. Suárez-Riestra, E. Martín-Gutiérrez, Perforated Board Shear Connector for Timber-Concrete Composites, Wood Materials Science & Engineering, 2022, https://doi.org/10.1080/17480272.2022.2089594.
[58] EN 1991-1-1, Eurocode 1: Actions on Structures, European Committee for Standardization, Brussels, 2002.
[59] EN 14080, Timber Structures. Glued Laminated Timber and Glued Solid Timber. Requirements, European Comittee for Standardization, Brussels, 2013, 2013.
[60] UNE 36068, Ribbed Bars of Weldable Steel for the Reinforcement of Concrete, Aenor, Madrid, 2011, 2011.
[61] EN 197-1, Cement. Part 1: Composition, Specifications and Conformity Criteria for Common Cements, European Committee for Standardization, Brussels, 2011, 2011.
[62] EN 14889-2, Fibres for Concrete. Part 2: Polymer Fibres. Definitions, Specifications and Conformity, European Committee for Standardization, Brussels, 2008.
[63] EN 12390-3, Testing Hardened Concrete. Part 3: Compressive Strength of Test Specimens, European Committee for Standardization, Brussels, 2019.
[64] EN 408:2010 +A1:2012, Timber Structures. Structural Timber and Glued Laminated Timber. Determination of Some Physical and Mechanical Properties, European Committee for Standardization, Brussels, 2012.
[65] EN 1995-1-1, Eurocode 5. Design of Timber Structures, European Committee for Standardization, Brussels, 2016.
[66] U.A. Girhammar, D.H. Pan, Exact static analysis of partially composite beams and beam-columns, Int. J. Mech. Sci. 49 (2) (2007) 239–255, https://doi.org/10.1016/j.ijmecsci.2006.07.005.
[67] U.A. Girhammar, A simplied analysis method for composite beams with interlayer slip, Int. J. Mech. Sci. 51 (2009) 515–530, https://doi.org/10.1016/j.ijmecsci.2009.05.003.

[68] EN 26891, Timber Structures. Joints Made with Mechanical Fasteners. General Principles for the Determination of Strength and Deformation Characteristics (ISO 6891:1983), European Committee for Standardization, Brussels, 1991, 1991.
[69] EN 1990:2002/A1: 2005. Eurocode. Basis of Structural Design, European Committee for Standardization, Brussels, 2005.
[70] EN 1995-1-1. Project team SC5.T3. Sub-task 7. Vibrations, in: Milestone 2, European Committee for Standardization, Brussels, 2019.
[71] M. Feldmann, et al., EUR 28084 EN. Design of floor structures for human induced vibrations, in: Background Document in Support to the Implementation, Harmonization and Further Development of the Eurocodes, Joint Research Centre, Institute for the Protection and Security of the Citizen. Publications Office of the European Union, 2011, https://doi.org/10.2788/4640.